Supplement Information

Design of ultra-stretchable, highly adhesive and self-healable hydrogels by tannic acid-enabled dynamic interactions

Jiaying Mo[1,4†], Yuhang Dai[1,2], Chao Zhang[1*], Yongsen Zhou[1,2], Wanbo Li[1,2], YuxinSong[1,2], Chenyang Wu[1,2,4] and Zuankai Wang[1,2,3,4*]

[1]Department of Mechanical Engineering, City University of Hong Kong, Hong Kong 999077, China
[2]Research Center for Nature-inspired Engineering, City University of Hong Kong, Hong Kong 999077, China
[3]Shenzhen Research Institute of City University of Hong Kong, Shenzhen 518057, China
[4]Health@InnoHK (Centre for Virology, Vaccinology and Therapeutics), Innovation and Technology Commission and Shenzhen Science, Hong Kong 999077, China.

**Corresponding Email: zuanwang@cityu.edu.hk*
† These authors contributed equally to this work

Part 1. Materials

Sodium chloride (NaCl, ⩾99.5%), sodium dibasic (Na_2HPO_4, ⩾99%) and potassium dihydrogen phosphate (KH_2PO_4, ⩾99.5%) were purchased from Meryer Co., Ltd. (Shanghai, China); Acrylic acid (AAc, 99%) was obtained from Sigma-Aldrich Co., Ltd. (Shanghai, China). Calcium chloride ($CaCl_2$, 97%) and tannic acid (TA, ACS reagent) were purchased from Alfa Aesar Chemical Co., Ltd. (Tianjin, China). 3-acrylamidophenylboronic acid (AAPBA) was obtained from Bidepharm medical technology Co., Ltd (Shanghai China). N,N'-methylenebisacrylamide (MBAA) was purchased from TCI (Shanghai) development Co., Ltd. All these reagents were used as received. A modified water-dispersible photoinitiator 2,4,6-trimethylbenzoyl-diphenylphosphine oxide (TPO) with high efficiency was synthesized as reported.[1] Polyvinyl chloride (PVC), glass, and aluminum (Al) plates are commercial products. Fresh pigskin was purchased from the local supermarket.

Part 2. Methods

2.1 Synthesis of TEDI hydrogels

We synthesized TEDI hydrogel using a facile one-pot polymerization method. Considering the fact that catechol and phenylboronic acid groups are prone to form borate ester bonds under a pH ranged from 7.4 to 8.5,[2] a phosphate buffer solution (pH = 7.46, 0.15 mol/ L, 37 ˚C) was selected and prepared by dissolving NaCl, Na_2HPO_4 and KH_2PO_4 in deionized water. Then, AAc monomer (2.04 mL, 5.95 mol/L) together with TA powder (8 wt% of AAc monomer) were added to 5 mL phosphate buffer and vigorously stirred for 3 min. Subsequently, $CaCl_2$ (5 wt% of AAc monomer), AAPBA powder (5 wt% of AAc) and highly efficient photoinitiator (TPO) were well dispersed in the precursor solution by ultrasonic dispersion for 15 min. After degassing in a vacuum chamber to remove oxygen in the solution, the precursor solution was injected

into the self-prepared molds (length × width × thickness = 30.0 mm×10.0 mm×3.0 mm) and placed under UV light (λ=365 nm) for 15 min within nitrogen protection. Finally, the as-fabricated hydrogels were immersed in aqueous solution to remove the unreacted residue. Note that the concentrations of AAPBA, TA and $CaCl_2$ can be used as parameters to adjust the amounts of dynamic borate ester bonds and noncovalent interactions.

As a control sample, the chemically crosslinked P(AAc-co-AAPBA) hydrogels were also fabricated via one-pot photopolymerization. The precursor solution was prepared in two steps. First, AAPBA powder (5 wt% of AAc) were dissolved in 5 mL aforementioned phosphate buffer solution with 5mL AAc monomer by ultrasonic dispersion. Then chemical crosslinking agent MBAA (1 wt% of AAc monomer) was added and then well dispersed under vigorous stirring at room temperature until the homogenous solution formed. After degassing in a vacuum chamber, the precursor solution was injected into molds and exposed to UV light to obtain the chemically crosslinked P(AAc-co-AAPBA) hydrogels.

2.2 Mechanical characterization

All mechanical tests were performed at room temperature using a servo control computer tensile testing machine. The uniaxial tensile test was performed on the rectangular-shape specimens (10 mm in width, 3 mm in depth, and 30 mm in length). The initial distance between two clamps was about 5 mm, and the constant stretching rate was controlled as 50 mm/min. The unconfined compression tests of the cylindrical sample (30 mm height and 20 mm diameter) were conducted at a crosshead speed of 50 mm min^{-1}. To evaluate the self-recovery ability, the specimen was initially stretched to a predetermined strain (100%) and then unloaded at the same velocity. Then, the successive loading-unloading tensile tests, with a speed of 50 mm min^{-1}, were conducted for four cycles without intervals between consecutive cycles. Similarly, the compression cycle tests with 80% strain were performed without resting as a measurement of compression hysteresis. The raw data were recorded as force versus

displacement and converted to stress versus strain with respect to the initial dimensions.

2.3 Characterization of structural morphology

The micromorphology of as-prepared TEDI hydrogel was characterized through scanning electron microscope (FEI Quanta 450 FESEM).

2.4 Self-adhesion characterization

To quantify the self-adhesion behaviors on different substrates, TEDI hydrogels were characterized by the lap-shear test. A hydrogel specimen with a thickness of 3 mm was sandwiched between two substrates with an overlapped area of 3.0*1.0 cm^2. The specimens were then pulled by a servo control computer tensile testing machine with a tensile speed of 10 mm min^{-1} until joint spilt. The adhesion strength was calculated by the maximum load divided by the initial bonded area.

2.5 Self-healing Test

Water-based dyes were added into precursor solution for better distinguishments. After gelation, the samples in shape of disks (1 cm in diameter and 5 mm in height) were cut into halves using razor blades. The cut surfaces were then brought together without applying external force and carefully sealed to retard water evaporation of hydrogels. After a fixed interval, the self-healed disks were stretched to straightly observe the self-healing performance. For further investigation, tensile tests are conducted to quantify the self-healing efficiency (SE) of hydrogels. The specimens (10 mm in width, 3 mm in depth, and 30 mm in length) were cut and healed in the mentioned condition. The self-healing efficiency was calculated based on the equation $SE = \frac{\sigma_{healed}}{\sigma_{uncut}} \times 100\%$, where σ_{healed} was the tensile stress of healed specimen, σ_{uncut} was the tensile stress of original specimen without cutting.

2.6 Electromechanical Test

The real-time electrical signals of the strain sensors based on the resistance changes of the hydrogels in a different state were recorded by sourcemeter after applying a fixed voltage of 3 V on the sensors. The hydrogel was deployed as channel material to fabricate strain sensors using the two-electrode configuration. Conductive metallic tapes were attached to the two ends of sensors and served as the electrodes also the barrier between hydrogel and clamps of tensile tester. To apply desired strains to the sensor for the electromechanical test, the motion of hydrogel was controlled by tensile tester through programming. Similar setups were employed for human motions monitoring.

Part 3. Tables and figures

Table S1. Comparison between recently reported mussel-inspired hydrogels with TEDI hydrogel.

Ref No.	Name of hydrogels	Maximum strain (%)	Adhesion strength on porcine skin (kPa)
11	GW-hydrogel	620	57
18	TA@CNC hydrogel	2900	5.2
21	PDA-clay-PAM hydrogel	4800	28.5
31	PL-Cat/Fe/ODex hydrogel	73	15
32	PSGO-PEDOT-PAM hydrogel	2000	20.5
33	NPs-P-PAA hydrogel	2660	27.5
34	P-0.08Al-0.3C-0.3T hydrogel	1850	23.5
35	PDA-PPy-PAM hydrogel	2200	30
36	DAL/rGO/SA/PAM Hydrogel	980	17.25
37	DTPAM hydrogel	1795	15.2
38	STP hydrogel	4000	15
39	MFH	800	12.6
this work	TEDI hydrogel	7338	49.81

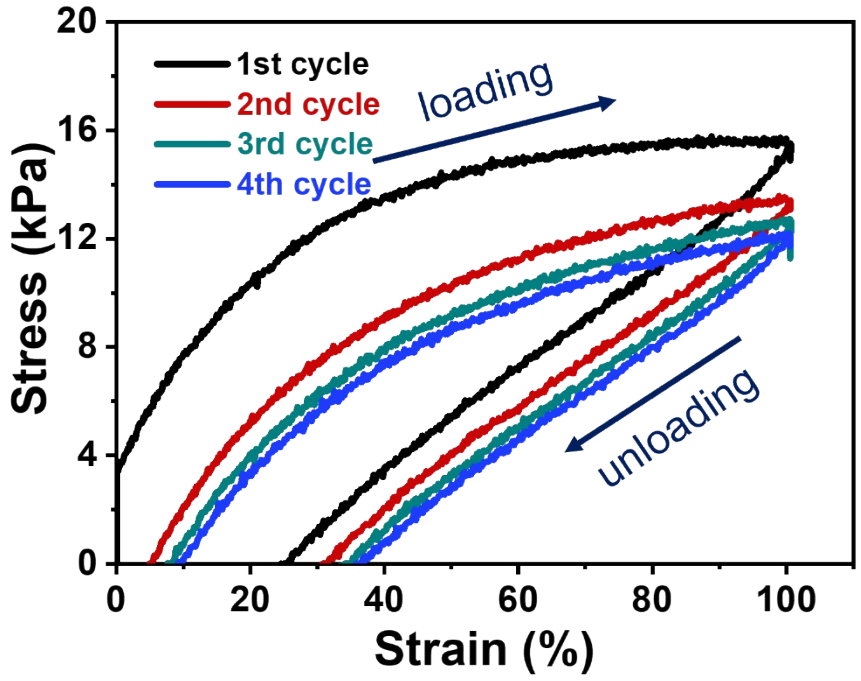

Figure S1. Continuous cyclic tensile loading–unloading curves at 100% strain without resting time between each cycle.

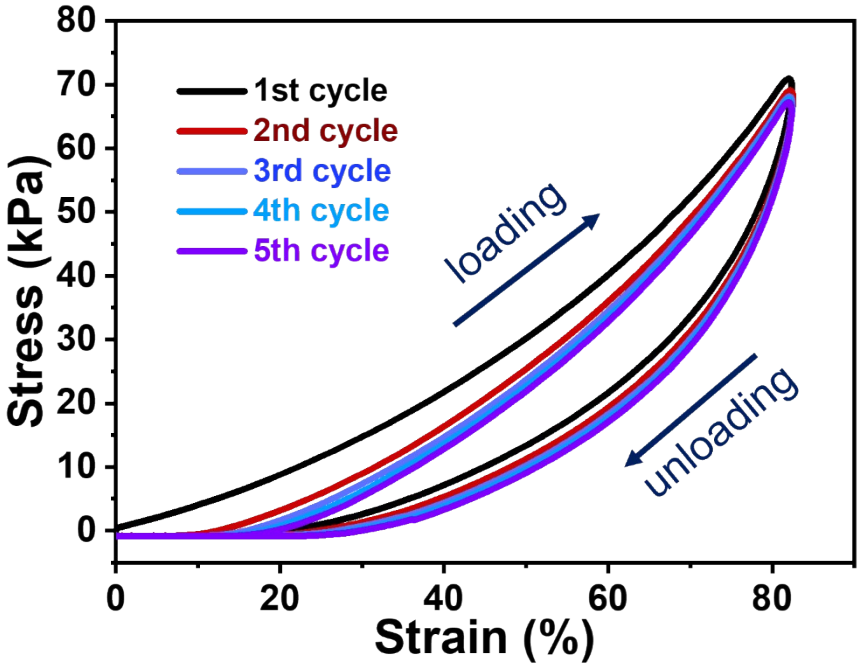

Figure S2. Typical successive loading−unloading compression tests of TEDI hydrogel 80% strain without resting intervals.

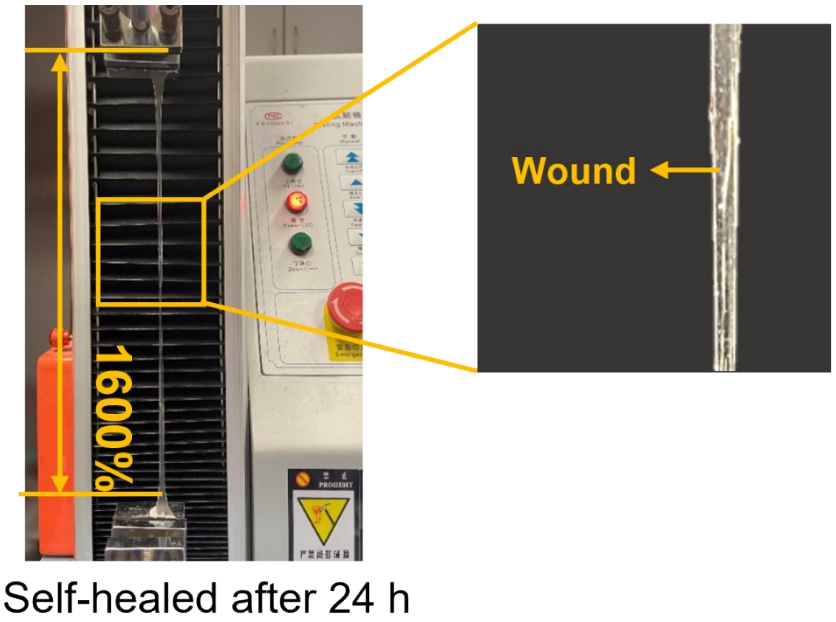

Figure S3. Self-healed TEDI hydrogel can be stretched to a strain of 1600% without any crack.

Table S2. Self-healing efficiency of TEDI hydrogel at different time.

Healing Time (h)	Maximum Strain (%)	Tensile Strength (kPa)	Self-healing Efficiency (%)
1	277.731	13.00	24.1
3	480.1	17.22	31.9
6	902.994	20.65	38.2
12	1157.494	24.06	44.56
24	1726.49	30.41	56.31
Original	7300	54	-

$Self-healing\ efficiency = \frac{\sigma_{healed}}{\sigma_{original}}$, where σ_{healed} is the tensile strength of healed specimens and $\sigma_{original}$ is the tensile strength of original specimen.

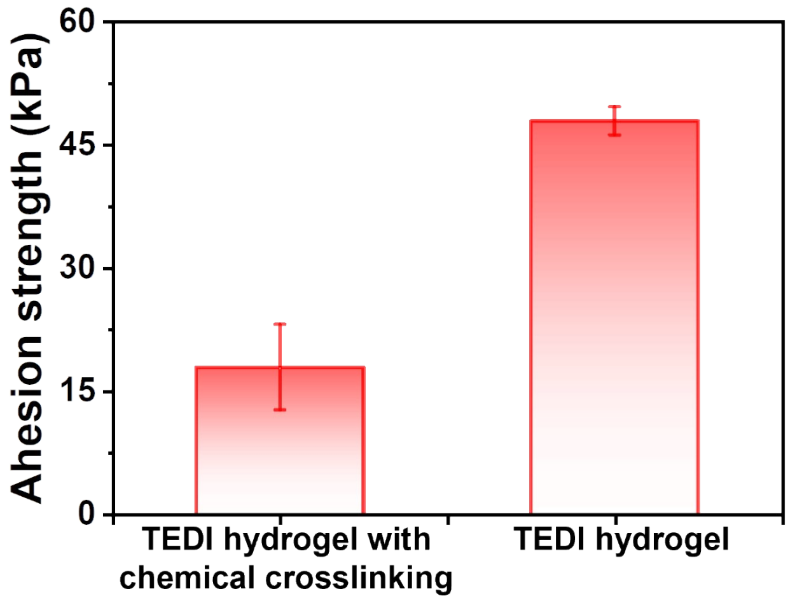

Figure S4. Comparison in terms of adhesion strength of fully dynamically crosslinked TEDI hydrogel and chemically crosslinked TEDI hydrogel. (concentration of MBAA: 1 wt% of AAc)

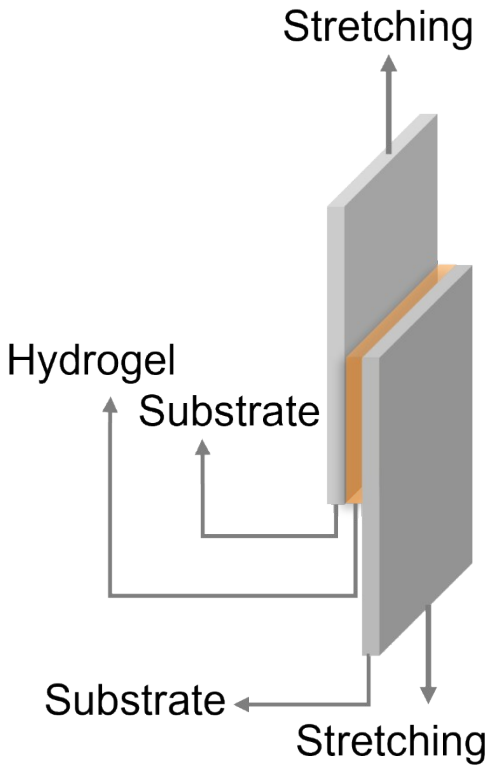

Figure S5. Schematic diagram of lap-shear adhesion test.

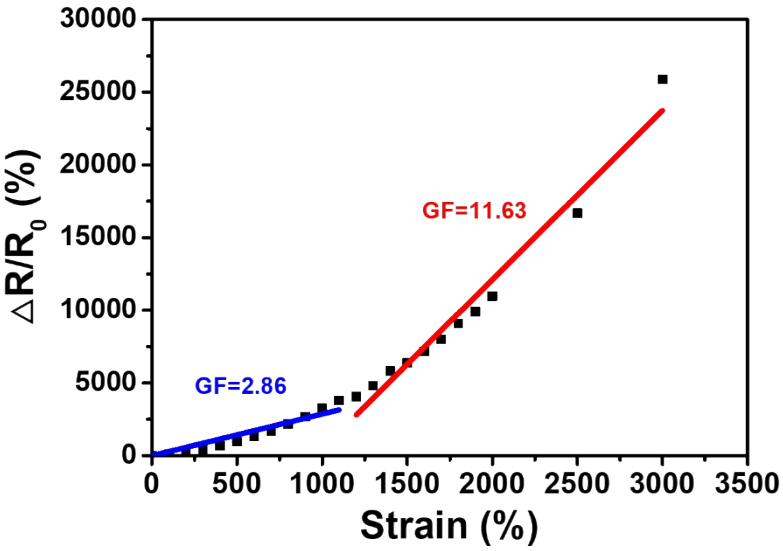

Figure S6. Time-dependent relative resistance changes of LiCl incorporated TEDI hydrogel sensor

Table S3. Comparison between recently reported hydrogel-based strain sensors with LiCl-integrated TEDI hydrogel in terms of gauge factor.

Ref No.	Name of hydrogels	Gauge factor (GF)
Ref 3, 4	LiBr-percolated PAM/carrageenan DN hydrogel	6 (0.47 without LiBr treatment)
Ref 5, 6	DCN hydrogel	343
Ref 7	CTPA hydrogel	12.2
Ref 8	CS-PHEAA DN-Cit hydrogel	6.9
Ref 9	MMCHs	8.5
This work	LiCl integrated TEDI hydrogel	11.63

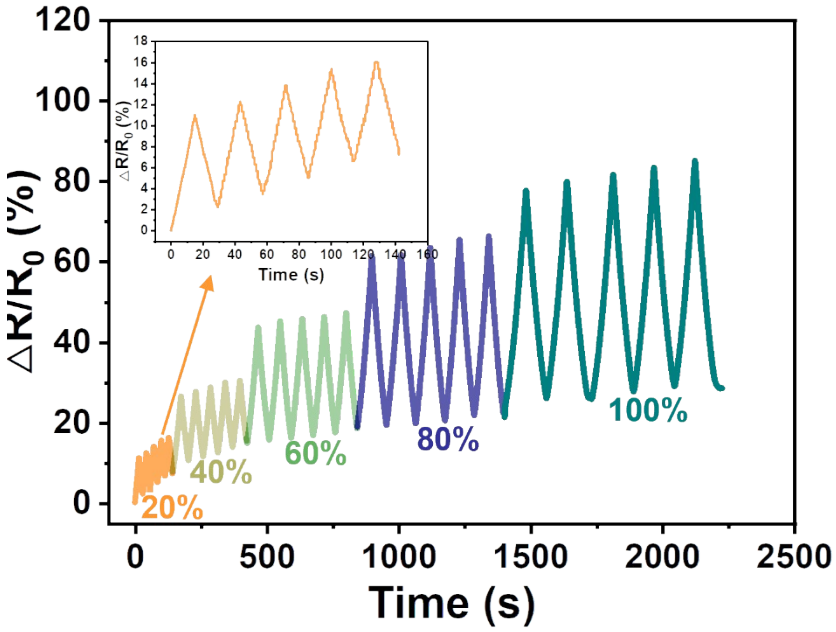

Figure S7. Time-dependent relative resistance changes of TEDI hydrogel sensor under strains in the range 20-100%.

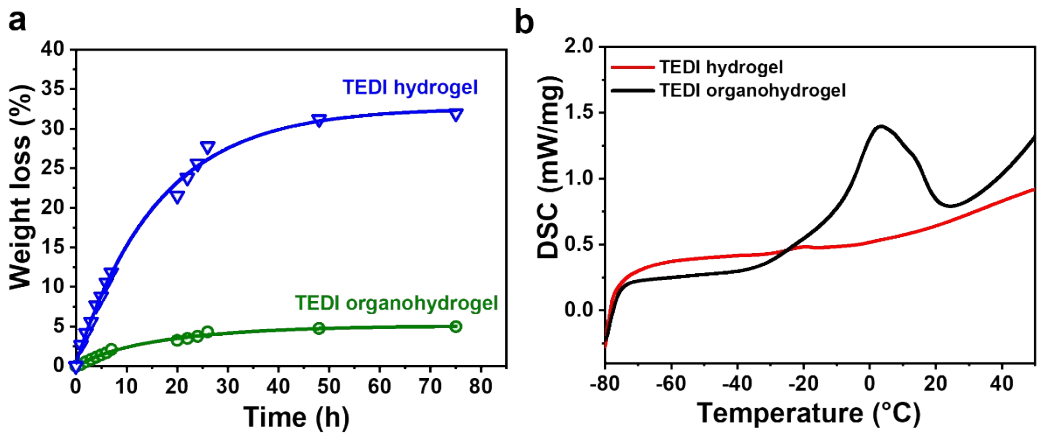

Figure S8. Anti-drying and anti-freezing properties of TEDI hydrogel after solvent replacement. (a) The relative change of the mass of the hydrogel with prolonged heating

at 50 ℃. (b) Differential scanning calorimetry (DSC) curve of TEDI hydrogel and hydrogel after solvent replacement. (Scan rate 10 ℃/min, in the first heating cycle).

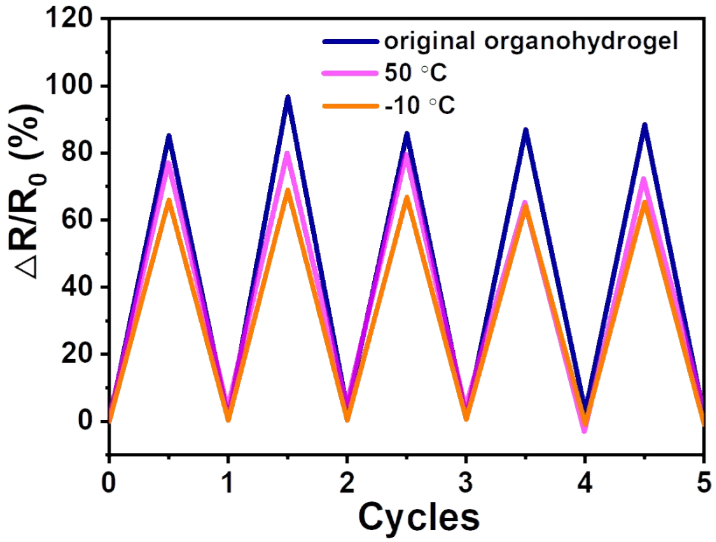

Figure S9 Stability of relative resistance changes for TEDI organohydrogel sensor in -10 ℃ and 50 ℃.

Part 4 References

1. A. A. Pawar, G. Saada, I. Cooperstein, L. Larush, J. A. Jackman, S. R. Tabaei, N. J. Cho, S. Magdassi, *Sci. Adv.*, 2016, **2**, e1501381.
2. Y. J. Chen, W. D. Wang, D. Wu, M. Nagao, D. G. Hall, T. Thundat, R. Narain, *Biomacromolecules*, 2018, **19**, 596-605.
3. J. Wu, Z. X. Wu, X. Lu, S. J. Han, B. R. Yang, X. C. Gui, K. Tao, J. M. Miao, C. Liu, *ACS Appl. Mater. Interfaces*, 2019, **11**, 9405-9414.
4. Z. X. Wu, W. X. Shi, H. J. Ding, B. Z. Zhong, W. X. Huang, Y. B. Zhou, X. C. Gui, X. Xie, J. Wu, *J. Mater. Chem. C*, 2021, DOI: 10.1039/D1TC02506F.
5. S. J. Han, C. R. Liu, X.Y. Lin, J. W. Zheng, J. Wu, C. Liu, *ACS Appl. Polym. Mater.*, 2020, **2**, 996-1005.
6. Z. X. Wu, X. Yang, J. Wu, J, ACS Appl. Mater. Interfaces, 2021, **13**, 2128-2144.
7. J. Y. Yin, S. X. Pan, L. L. Wu, L. Y. N. Tan, D. Chen, S. Huang, Y. H. Zhang, P. X. He, *J. Mater. Chem. C*, 2020, **8**, 17349-17364.
8. Y. Y. Yang, Y. T. Yang, Y. X. Cao, X. Wang, Y. R. Chen, H. Y. Liu, Y. F. Gao, J. F. Wang, C. Liu, W. J. Wang, J. K. Yu, D. C. Wu, *Chem. Eng. J.*, 2021, **403**, 126431.
9. H. L. Sun, Y. Zhao, S. L. Jiao, C. F. Wang, Y. P. Jia, K. Dai, G. Q. Zheng, C. T. Liu, P. B. Wan, C. Y. Shen, *Adv. Funct. Mater.*, 2021, **31**, 2101696.
10. G. Ge, Y. Z. Zhang, J. J. Shao, W. J. Wang, W. L. Si, W. Huang, X. C. *Adv. Funct. Mater.*, 2018, **28**,1802576.